Estuaries and Coasts (2025) 48:19
https://doi.org/10.1007/s12237-024-01438-4

Impacts of the Seasonal Migration of an Estuarine Turbidity Maximum on Local Hydrodynamics and Mixing in the Ems Estuary

T. Bailey[1] · L. Ross[1] · H. M. Schuttelaars[2] · D. S. van Maren[3,4]

Received: 3 June 2024 / Revised: 21 August 2024 / Accepted: 26 September 2024

Abstract

This study examines the local, intratidal effects of suspended sediment concentrations (SSCs) on the hydrodynamics and vertical mixing in the Ems Estuary, located on the border between Germany and The Netherlands, during summer and winter seasons when the estuary turbidity maximum (ETM) is located upstream and adjacent to the study site, respectively. Measurements of density, SSCs, turbulent kinetic energy dissipation, and current velocity were collected and analyzed over a semi-diurnal tidal cycle in August of 2018 and January of 2019 as part of the collaborative Ems-Dollard Measurement (EDoM) campaign. During August, the estuary turbidity maximum was located 25 km upstream from the measurement site and local SSCs were low. Results revealed that under these conditions, suspended sediment minimally impacted vertical mixing by stabilizing density near-bottom during flood tide, while typical salinity-induced tidal straining patterns dominated. During January, the ETM was located only 5 km upstream of the measurement site leading to higher local sediment concentrations. Salinity-induced straining of the density occurred on early flood tide, creating stratification that suppressed vertical mixing. The suppression was enhanced by the contribution of vertical gradients in SSC to density, as signified by the gradient Richardson number. Suppression of vertical mixing by sediment-enhanced stratification was most significant within the hour following maximum flood currents when elevated velocity shear occurred. The variability observed between the local dynamics during August and January were attributed to greater sediment concentrations due to the ETM proximity in January. The intratidal asymmetry of vertical mixing observed under higher SSCs likely has implications for sediment transport.

Keywords Estuary · Suspended sediment concentration · Mixing · Sediment-induced stratification · Ems Estuary

Communicated by Hui Wu

Key Points
- Variability in the along-channel position of an estuary turbidity maximum impacts local mixing dynamics.
- Sediment concentration gradients enhance density stratification and suppress mixing in the water column.
- Strongest sediment-enhanced stratification during flood tide in winter inhibits mixing.

✉ L. Ross
lauren.ross1@maine.edu

[1] Department of Civil and Environmental Engineering, University of Maine, Orono, ME, USA

[2] Delft Institute of Applied Mathematics, Delft University of Technology, Mekelweg 4, 2628 CD Delft, The Netherlands

[3] Coastal and Marine Systems, Deltares, Delft, South Holland, Netherlands

[4] Environmental Fluid Mechanics Section, Delft University of Technology, Delft, South Holland, The Netherlands

Introduction

In highly turbid estuaries, suspended sediment concentrations (SSCs) can contribute to density and affect vertical mixing by altering stratification (Dyer et al. 2004; Zhu et al. 2021; Becker et al. 2018). However, the dynamics that lead to sediment-induced density stratification along with when and where within the estuary it is expected to occur, have received little attention. This is particularly true at relatively low sediment concentrations when compared to fluid mud conditions (minimum concentrations of 10 kg/m^3; Ross 1988). Van der Ham et al. (2001) was one of the first studies that collected high-frequency measurements of velocity and sediment for the purpose of investigating the influence of sediment-induced stratification on turbulence. Their observations in the Ems Dollard showed that sediment-induced stratification had little significance near the bed in shallow tidal channels, but they emphasize a need for future investigations above the bed. In contrast, Scully and Friedrichs

Published online: 15 November 2024

(2003) later hypothesized that increased near-bed sediment gradients caused a reduction of turbulence during flood tide in the York River. This was evidenced by a reduction of the bottom drag coefficient on flood tide (compared to ebb) despite comparable vertical salinity gradients between the two tidal phases. However, the presence of sediment-induced stratification during flood tide in the York River remained speculation due to insufficient measurements. There remains a need to understand what local field conditions and dynamics are conducive to sediment gradients that will impact vertical mixing for accurate sediment transport modeling and predictions.

A study by Tu et al. (2019) observed intratidal asymmetry in sediment-induced stratification under high sediment concentrations (up to 15 g/L near the bed) in the Qiantang Estuary in China, finding stronger sediment-induced stratification on flood tide. Despite this, they also observed greater turbulence on flood tide, which was speculated to be a result of horizontal advection of turbulent dissipation into the measurement location. Tu et al. suggested that the effect of sediment-induced stratification on turbulence may increase with distance from the bed but were not able to prove this. In conditions of fluid mud in the Ems Estuary, Becker et al. (2018) showed that there exists a dynamic feedback loop between the effects of mud-induced periodic stratification on the flow and intratidal asymmetries in velocity shear and mud transport. They note that in hyperturbid systems, SSC, not salinity, controls the local density, and thus the stratification (Becker et al. 2018). Their study discussed the role of mixing, using the tightness of isolutols as a proxy, on destratification of the water column. It remains to be investigated if the findings of Becker et al. (2018) are applicable at lower sediment concentrations, that is, in the absence of fluid mud and under conditions where both salinity and sediment concentrations influence density.

Other studies have focused on the impact of sediment gradients on vertical mixing within the estuary turbidity maximum (ETM) (Zhu et al. 2021; Lu et al. 2020). The along-channel location of an ETM typically exhibits seasonal variability (De Jonge et al. 2014; Burchard et al., 2018, and references therein), thereby impacting the availability of sediment supply to locations downstream. The Ems River is an example where the along-channel position of the ETM can vary by more than 20 km due to seasonal variations in river discharge (De Jonge et al. 2014). Although the mixing dynamics in the hyperturbid upper portion of the river have received attention (Becker et al. 2018; Winterwerp et al. 2017; Winterwerp 2011), the consequences of variation in the along-channel ETM location on the hydrodynamics, in particular mixing, at locations downstream remain relatively unexplored (van Maren et al. 2023). Therefore, the overarching goal of this study is to better understand how the seasonal migration of an upstream ETM affects the current velocities, stratification, and vertical mixing dynamics at intratidal scales downstream. To reach this goal, two specific questions will be answered: 1) How does the along-channel location of the ETM impact density at a downstream location, and 2) how do these impacts manifest in the local hydrodynamics and vertical mixing dynamics at intratidal scales? These research questions will be answered through analysis of data collected during the Ems-Dollard Measurements (EDoM) joint German-Dutch field campaign that took place in the Ems Estuary in August of 2018 and January of 2019. During the EDoM campaign, measurements were collected at several fixed locations along the Ems Estuary, one of which is the focus of this study and will be elaborated upon more in Study Site. Methods will present methodologies for data collection and analysis, including processing of current velocity and microstructure profiles as well as the conversion of the measured turbidity to suspended sediment concentrations. Results are presented in Results and discussed in Discussion focusing on how the seasonal variation in sediment-induced stratification alters mixing and flow regimes downstream. In Conclusions conclusions will be drawn.

Study Site

The Ems Estuary in general is a partially- to well-mixed, semidiurnal, flood-dominant system (Dyer et al. 2000). It is mesotidal with a tidal range of approximately 3.5 m (Talke et al. 2009). The primary source of freshwater into the Ems Estuary is the portion of the Ems River upstream of the weir at Herbrum, which has an average discharge of 70 m^3/s measured at Versen (40 km upstream of the Herbrum weir). The Ems River has seasonal variations in discharge from 10 m^3/s to above 600 m^3/s (De Jonge et al. 2014). Brackish water can reach as far upstream as Papenburg (Fig. 1a) under low freshwater discharge conditions (Talke and de Swart 2006). Seasonal variations in river discharge have been found to influence the location of the ETM within the lower Ems River. De Jonge et al. (2014) showed that during the late fall (November) of 2005, river discharge increased from 40–60 m^3/s to 100–150 m^3/s in the winter. As a result, the ETM, with near-surface SSCs on the order of 2–3 kg/m^3, was advected from ~ 5–10 km from the weir at Herbrum to ~ 35–50 km downstream from the weir. Part of the Ems Estuary consists of a 12 km long fairway providing access to the port of Emden, which is sheltered from the mudflats of the Dollard Bay along its southern boundary by the semi-permeable Geise Dam (Talke and de Swart 2006). The results from De Jonge et al. (2014) suggest that when the river discharge exceeds 70 m^3/s sediment trapped within the ETM can be flushed into the fairway and the lower Ems Estuary reaching the port of Emden, as it is ~ 54 km from the weir at Herbrum,

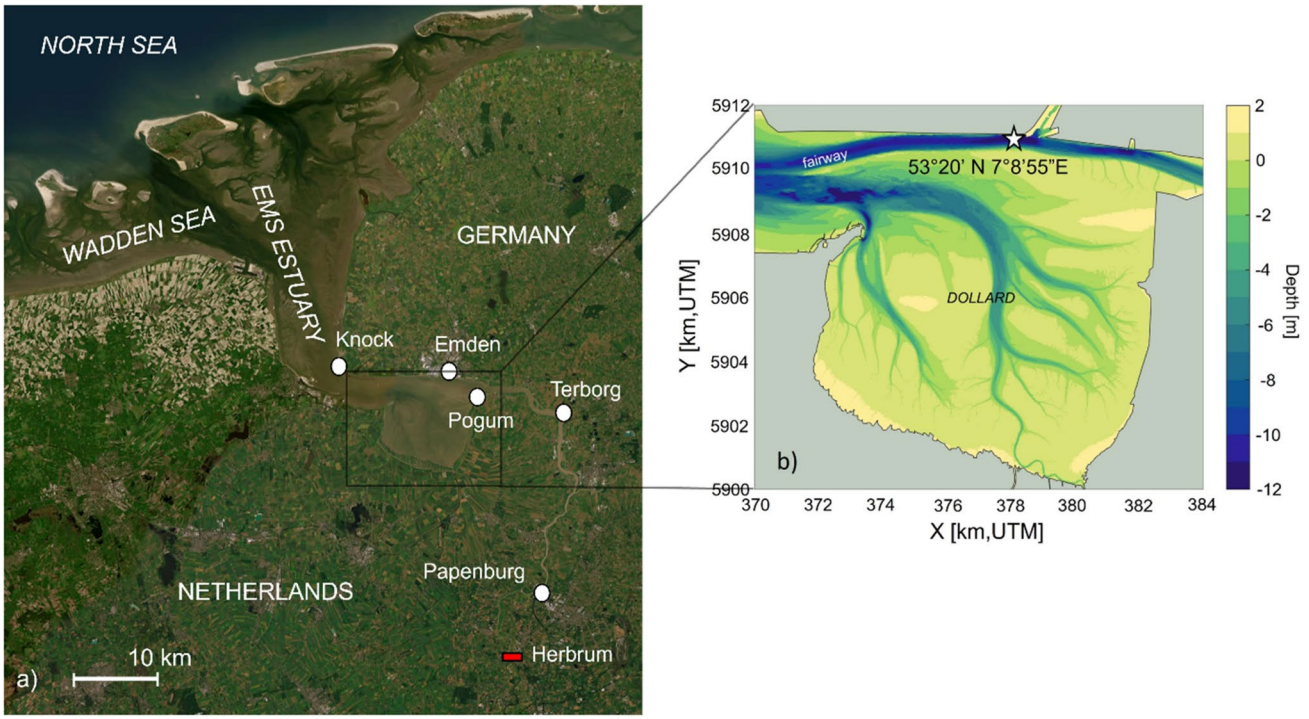

Fig. 1 **a**) The study area in relation to the Netherlands and Germany. The weir at Herbrum is located approximately 54 km upstream from Emden. Salinity intrusion can reach up to Papenburg. **b**) Bathymetry within the Dollard. The measurement location within the fairway is marked with a star and the coordinates of the measurement site. Image Credit: Esri (2024)

having major consequences on infill and planned dredging activities for the port. Both the Ems Estuary and the lower Ems River have become increasingly turbid over the past few decades, due to a combination of channel deepening effects on tidal asymmetry (Chernetsky et al. 2010; Winterwerp et al. 2013; De Jonge et al. 2014; Dijkstra et al. 2019) and gravitational circulation (van Maren et al. 2015a) in combination with reduced flushing (van Maren et al. 2015b; Winterwerp et al. 2017) and loss of sediment sinks (van Maren et al. 2015a, 2016). It is therefore important to understand linkages between ETM migration and hydrodynamics in the fairway that connects the upper and lower Ems Estuary.

The majority of sediment in the Ems Estuary is comprised of sand and fine-grained sediments of marine origin, imported from the Wadden Sea and the North Sea (Van Maren, et al. 2015a, b; Winterwerp et al. 2017). Flocculation of fine-grained suspended sediments near Emden have been shown to produce macroflocs around 200 mm in size (van Leussen 2011). In the lower Ems River, fine-grained sediments consolidate into fluid mud reaching concentrations up to 200 kg/m^3 (Papenmeier et al. 2013). Fluid mud (minimum concentrations of 10 kg/m^3) in the lower Ems River has been observed to extend nearly as far downstream as Gandersum and upstream beyond Papenburg (Talke et al. 2009).

Methods

The measurements collected for this study were part of the large-scale Ems-Dollard Measurement (EDoM) campaign that took place in August 2018 and January 2019 to capture the summer and winter seasons, respectively. The overall goal of the EDoM campaign was to better understand the driving mechanisms of water and sediment exchanges between the lower and upper Ems Estuary to finally pinpoint the drivers of the consistent sediment accumulation in the upper estuary and how this affects sediment concentrations and hydrodynamics in the lower river. The overall campaign included eight research vessels and 10 moorings that collected measurements for at least one semidiurnal tidal cycle. The measurements examined in this study were collected at a strategic location at the transition between the hyperturbid upper Ems Estuary and the turbid lower estuary near Emden (Fig. 1) to shed light on how the seasonal along-channel migration of the ETM affects local hydrodynamics, mixing, and sediment transport. The location of the study site was downstream of the ETM during summer (August) and at the toe of the ETM during winter (January) (van Maren et al. 2023). This will be elaborated upon more in the following section.

Data Collection

During the EDoM campaign, salinity and turbidity were measured along the Ems Estuary and lower Ems River during an along-channel cruise. The details of this cruise are described in van Maren et al. (2023) and the measurements of along-channel turbidity and salinity are shown in their Fig. 4 (not shown here). The measurements from van Maren et al. (2023) show that the ETM was located further downstream by approximately 25 km during the January 2019 campaign compared to the August 2018 campaign. In August, the toe of the ETM was ~ 20 km downstream of Papenburg whereas it was ~ 35 km from Papenburg in January, which is very near to Emden, the site where data was collected for this study (Fig. 1).

For this study, current velocity data were collected throughout a semidiurnal tidal cycle (~ 12 h) close to spring tide conditions from a stationary boat (fixed point) anchored near Emden at approximately 53°20′0.26″N, 7°8′55.27″E in the Ems Estuary (Fig. 1) on August 28, 2018 and January 24, 2019. The stationary boat was equipped with a downward facing 600-kHz RDI Workhorse Acoustic Doppler Current Profiler (ADCP) which collected horizontal velocities throughout the water column in the east–west, u, and north–south, v, directions. The ADCP bin size was 0.5 m, and the sampling rates used in August and January were 1 Hz and 2 Hz, respectively.

A second research vessel collected turbidity, salinity, temperature, and velocity shear via a Rockland Scientific MicroCTD as close as possible to the stationary and anchored vessel that held the ADCP. Turbidity and velocity shear, the latter of which was collected by two accelerometer probes located on the top of the instrument, were measured at a rate of 512 Hz and salinity and temperature were measured at 64 Hz. The fall velocity of the instrument was maintained as close to 0.8 m/s as possible as instructed by the manufacturer. The MicroCTD was deployed off a second vessel and not the same stationary boat as the ADCP since the instrument must drift with the currents with no tension in the rope. The objective was to collect 5 vertical casts every 15 min at a fixed location to obtain one representative and statistically significant profile. A total of 160 and 125 casts were performed in August and January, respectively. The MicroCTD velocity shear data were post processed to provide direct estimates of ε via a fit of the shear measurements to a theoretical Naysmyth spectrum (Ross et al. 2019; Douglas et al. 2018, and references therein).

Wind data were available from the German Weather Service station 5839 (53.39°N, 7.23°E; https://opendata.dwd.de) for January 2019, from which it was concluded that winds were not strong enough to induce significant mixing during this survey (not shown). Conditions on August 28, 2018, were also considered calm (Schulz et al. 2020). Water level measurements were provided by the Waterways and Shipping Office in Emden (WSA), as were river discharge values measured at the Versen monitoring station.

Data Analysis

Velocities, Mixing, and Hydrographic Data

The horizontal velocities (u and v) collected by the ADCP were averaged every 5 min and were rotated using a regression analysis (Thomson and Emery 2014) to their primary axis directions (along-channel and cross-channel). All other hydrographic data collected by the MicroCTD (salinity, temperature, density, turbidity) were averaged over 2 s intervals with 50% overlap to be consistent with the ε grid (Lueck et al. 2020). It should be noted that data from the MicroCTD were only used for post-processing and analysis when the instrument fall velocity was within ± 0.15 m/s of the required 0.8 m/s, when the angle of descent was less than ± 5 degrees, and the depth was at least 1 m. These criteria required the removal of data from the first ~ 3 m of the water column and the bottom ~ 1 m. The values of ε themselves were quantified using the method developed by Rockland Scientific (see Supplementary Information for more details). Then, a bootstrap of the data casts performed within the 15-min windows was calculated, resampling 6000 times to provide one statistically significant profile varying with depth for ε (Efron and Gong 1983; see Supplementary Information for further details). All other variables collected with the MicroCTD were averaged over all casts performed within the 15-min to provide one time-averaged vertical profile. If less than two casts within each 15-min set were measured at a particular depth, the data at that depth for that particular cast was neglected to reduce bias induced by a single measurement. These time-averaged profiles, the ε profiles, and the time-averaged profiles of the velocity data were interpolated onto consistent time and depth grids, with 5-min spacing and 0.5 m vertical bins, for calculation of the mixing parameters.

Mixing Parameters

Several parameters were used to determine links between suspended sediment concentrations and mixing. Using the methodology of Kay and Jay (2003) as outlined by Huguenard et al. (2015) and Spicer and Huguenard (2020), vertical eddy diffusivity (K_z) and vertical eddy viscosity (A_z) were quantified, respectively, as,

$$K_z = \Gamma_{mK} \frac{\varepsilon}{N^2} \tag{1}$$

$$A_z = \Gamma_{mA} \frac{\varepsilon}{S^2} \tag{2}$$

where N^2 is the squared buoyancy frequency,

$$N^2 = -\frac{g}{\rho_o}\frac{\partial \rho}{\partial z}, \tag{3}$$

g is the acceleration of gravity, ρ_o is the background (mean) density, and ρ is the water density. In Eq. 3, $S^2 = (\partial u/\partial z)^2 + (\partial v/\partial z)^2$ is the squared vertical shear. The mixing efficiency factor of K_z, Γ_{mK}, is quantified as $\Gamma_{mK} = Ri_f(1 - Ri_f)^{-1}$, and the mixing efficiency factor of A_z, Γ_{mA}, is quantified as $\Gamma_{mA} = (1 - Ri_f)^{-1}$. In these formulations, Ri_f is the flux Richardson number, equal to the Richardson number, $Ri = N^2/S^2$, divided by the nondimensional turbulent Prandtl number, Pr_{turb}. A value of $Ri > 0.25$ is often considered indicative of total suppression of shear-driven mixing due to density stratification (Miles 1961). According to Tjernstrom (1993), the turbulent Prandtl number can be quantified as,

$$Pr_{turb} = \sqrt{1 + 4.47Ri} \tag{4}$$

for stably stratified flows. It is also the case that Pr_{turb} is equal to the ratio of K_z and A_z. In the calculation of Ri_f, an upper limit of 0.18 was imposed following Osborn (1980) as it is anticipated that turbulence cannot be maintained at steady state above this threshold (Spicer and Huguenard 2020).

Suspended Sediment Concentrations

Turbidity measurements collected from the MicroCTD were converted to SSC using in-situ collected measurements. A linear regression model was used for this conversion to reduce uncertainty in the relation between turbidity and SSC (Fettweis et al. 2019). The coefficient of determination (R^2) value was 0.94 using this model for the January 2019 data, but the relationship was weaker for August 2018 ($R^2 \approx 0.45$) due to small concentrations of SSC (see Supplementary Information, Figure S2). According to Fettweis et al. (2019), $R^2 > 0.9$ is necessary to reduce prediction bias associated with outliers in the data set. The model equation used for conversion was therefore based on January 2019 data only, an approach similar to that of Tu et al. (2019).

The SSC measurements were used to calculate density of the sediment–water mixture (including the influence of salinity, temperature, and sediment) using the equation from Guan et al. (2005):

$$\rho_{SSC} = \rho + SSC\left[\frac{\rho_s - \rho}{\rho_s}\right] \tag{5}$$

where ρ_s is the sediment density. Values of $\rho_s = 2534.9$ kg/m^3 and 2541 kg/m^3 were obtained from bottom samples for August 2018 and January 2019 respectively for use in Eq. 5. Water density, calculated from salinity and temperature measured by the MicroCTD using the Gibbs-SeaWater Oceanographic Toolbox (based on the Thermodynamic Equation of Seawater – 2010, McDougall and Barker 2011), was used in Eq. 5 for ρ. For the remainder of this paper, the subscript *SSC* will be used to denote a parameter calculated using density as expressed in Eq. 5. If no subscript is present, this indicates that the density used considers salinity- and temperature-effects only.

Results

Hydrodynamic Conditions

August 2018

During the measurement campaign on August 28, 2018 discharge from the Ems River was ~ 22 m^3/s as measured at the monitoring station at Versen (Schulz et al. 2020). At this time, the ETM was located in the lower Ems River, with the downstream boundary of the ETM approximately 25 km upstream from the measurement site (Fig. 4 in van Maren et al. 2023). The measurements collected as part of this study began at the end of ebb tide (Fig. 2). Peak flood velocities of ~ 1.1 m/s occur between ~ 9–10.5 h near-surface (Fig. 2a). Sediment resuspension during peak flood velocities creates a vertical difference in SSC of ~ 1 kg/m^3 from bottom to surface, with maximum SSCs reaching approximately 1.2 kg/m^3 (Fig. 2e). The timing of sediment suspension coincides with peak flood velocities and higher levels of ε (~ 10^{-5} W/kg) extending from near bottom to ~ 2 m below the water surface (Figs. 2a,e,g). This is further evidenced by the depth location of the maximum vertical gradient of SSC (shown as dots in Fig. 2e-g). At peak flood, N^2_{SSC} is also elevated due to straining of the isohalines near-surface (Fig. 2d) and by the sediment gradient in the mid-water column. When sediment is not considered in the density, N^2 (not shown) is negative in some parts of the lower water column where sediment is suspended. This indicates that the sediment acts to stabilize the density, as a negative N^2 indicates instability. Stronger S^2 coincides with greater ε at the start of flood tide (~ 9 h, Figs. 2g and 2f, respectively), with S^2 reducing from 9–11 h while ε remains elevated. This could be due to the cross-channel velocities advecting elevated ε to the study site at this time (Fig. 2b and g), or rather the fact that near-bottom data is missing from the current-velocities that could indicate larger S^2 values than those in the upper water column. During high water slack tide (~ 13–14 h), S^2 and ε are reduced ultimately reducing SSC because of reduced suspension by tidal shear combine with settlement under weaker currents. The maximum values of ε during flood tide occur when the maximum vertical gradient of SSC is near

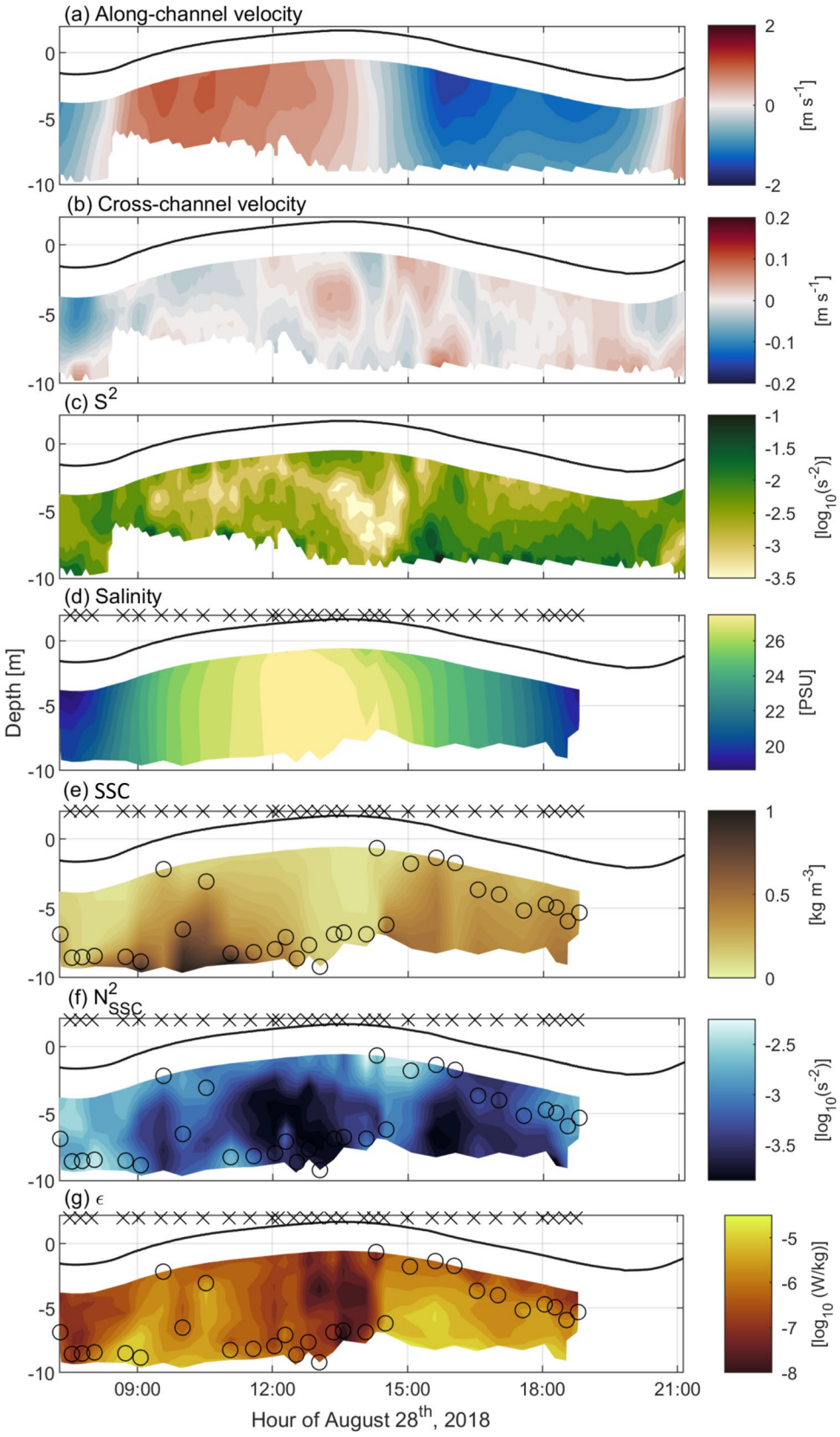

Fig. 2 With depth on the vertical axis and the hour on August 28, 2018, on the horizontal axis: (**a**) Along-channel velocity. Positive values represent inflow; negative values represent outflow. (**b**) Cross-channel velocity. Positive values represent flow toward the northern riverbank; negative values represent flow toward the Geise Damm. (**c**) Vertical Shear Squared. (**d**) Salinity. (**e**) Suspended sediment concentrations where the dots indicate the depth of the maximum vertical gradient of SSC. (**f**) Buoyancy frequency including effects of SSC with the location of the maximum vertical gradient in SSC shown as the dots. (**g**) Turbulent kinetic energy dissipation with the location of the maximum vertical gradient in SSC shown as the dots. The x's at the top of panels (d-g) denote times of the MicroCTD casts

surface, indicating that the velocity shear is sufficiently large to homogenize the water column in both density and sediments, allowing for the turbulent boundary layer to extend to the surface.

During ebb tide (~ 14–20 h), maximum current velocities of ~ 1.6 m/s occur near-surface at ~ 16 h (Fig. 2a). Bottom-generated shear enhances ε, but despite comparable current magnitudes in the lower water column, sediment concentrations are not as high as during flood tide, reaching only ~ 0.5 kg/m^3 (Fig. 2e-f). However, the maximum vertical gradient in SSC remains at the surface throughout ebb tide indicating a homogenized sediment concentration (Fig. 2e). Straining of the isohalines (Fig. 2d) causes strong N^2_{SSC} near-surface (< 3 m) during early ebb (~ 15 h; Fig. 2h), but around the same time strong currents increase S^2 and ε in the lower water column. Both S^2 and ε remain elevated throughout ebb tide and continuously suspend low concentrations of sediment (< 0.5 kg/m^3), which results in a more homogenous water column during ebb than flood. Overall, the dynamics throughout the August tidal cycle resemble strain induced periodic stratification (SIPS) (Simpson et al. 1990), with enhanced stratification during ebb.

January 2019

During the field campaign on January 24, 2019 the river discharge was higher relative to the August 2018 campaign, measuring ~ 60 m^3/s. Under these conditions, the ETM extended into the fairway, with the downstream boundary within approximately 5 km of the measurement site (van Maren et al. 2023). Higher SSCs, exceeding 3.5 kg/m^3 near bottom (Fig. 3e), nearly three times greater than observed during August (Fig. 2e), are observed due to the proximity of the ETM.

Suspended sediment concentrations are high (> 3 kg/m^3) throughout the water column during low water slack tide (Fig. 3e), decreasing gradually into early flood tide (~ 9.25–10.5 h; Fig. 3a). Such high concentrations of sediment throughout the water column prior to flood tide are from the downstream advection of sediment from the ETM, or possibly the ETM itself, which is known to experience tidal modulation in its along-channel position (Winterwerp et al. 2017). The SSC is quickly reduced in the mid-water column near peak flood (~ 10.5 h), due to upstream advection of suspended sediment caused by subsurface maximum flood current velocities (~ 1.9 m/s) (~ 10.5 h; Fig. 3a). Shortly after (~ 11 h), S^2 values increase (Fig. 3c), locally suspending sediment and producing a noticeable vertical gradient between ~ 7–9 m depth. Despite high S^2, ε is not elevated above depths of ~ 7 m (Fig. 3g) until the along-channel velocity is reduced to < 1.3 m/s (~ 12.5 h; Fig. 3a). Near bottom, sediment gradients (Fig. 3e) contribute to the density, creating a layer of stratification (high N^2_{SSC}) that confines ε to depths below ~ 7 m (Fig. 3f), which is evidenced by the depth location of the maximum vertical gradient in SSC remaining below 5 m depth (dots in Fig. 3e-g). Despite the presence of high salinity water above lower salinity water in this region at max flood, and in the midwater column during late flood (~ 13.5 h; Fig. 3d), the water column is stably stratified by the sediment gradient.

The observed vertical gradients in SSC are well-established until the end of flood tide (~ 15 h), after which suspended sediment likely settles under weak currents during high water slack. During early ebb (~ 17 h; Fig. 3b), ε appears to again be confined to the near bottom (> 7 m) despite strong S^2. This is speculated to be a result of an elevated gradient in SSC near-bottom, in the region below which the measurements capture, generated by resuspension of sediment via strong S^2. An interpolation of the salinity field from 16.5 h to 19 h was carried out due to lost salinity measurements from instrument interference with the bottom (red x's in Fig. 3d and f mark location of interpolated data).

During mid-to-late ebb (~ 18.5–20 h) the salinity shows straining of the isohalines (Fig. 3d), which causes increased N^2_{SSC} (Fig. 3h) throughout the water column. Despite relatively high buoyancy, ε is elevated throughout the water column. During ebb, maximum current velocities are weaker than during flood (~ 1.6 m/s) but occur near-surface and are sustained for several hours (~ 17–20.5 h). The high near-surface currents cause elevated S^2 that extends to the surface over ~ 18–20 h (Fig. 3g). The elevated shear likely outweighs the buoyancy effects during ebb, allowing ε to extend to the surface (Fig. 3f), but the balance between shear-induced mixing and stratification will be discussed later with the gradient Richardson number (see January 2019). Toward the end of ebb (~ 20–21 h) sediment becomes elevated again throughout the water column, reaching ~ 3.5 kg/m^3, due to sediment sourced from the ETM (similar to the start of the time series, 9–10 h).

Temporal Variations in Vertical Mixing

August 2018

During slack tides (~ 8–9 h and ~ 13–14 h), the depth-averaged vertical gradient of ρ_{SSC}, $\langle \frac{\partial \rho_{SSC}}{\partial z} \rangle$ (where angle brackets denote a depth average), increased primarily due to salinity-gradients ($\langle \frac{\partial \rho}{\partial z} \rangle$, Fig. 4a). Contributions to $\langle \frac{\partial \rho_{SSC}}{\partial z} \rangle$ from sediment gradients, quantified as the depth-averaged vertical gradient of density quantified without the effects of salinity (ρ_{nosalt}), $\langle \frac{\partial \rho_{nosalt}}{\partial z} \rangle$, are minimal due to low sediment concentrations (< 0.5 kg/m^3, Fig. 4a). Sediment contributes most to $\langle \frac{\partial \rho_{SSC}}{\partial z} \rangle$ on flood tide when the most sediment is in suspension and $\langle \frac{\partial \rho_{SSC}}{\partial z} \rangle$ and $\langle \frac{\partial \rho_{nosalt}}{\partial z} \rangle$ are nearly equal. The difference between the density computed with and without SSC (ρ_{SSC}

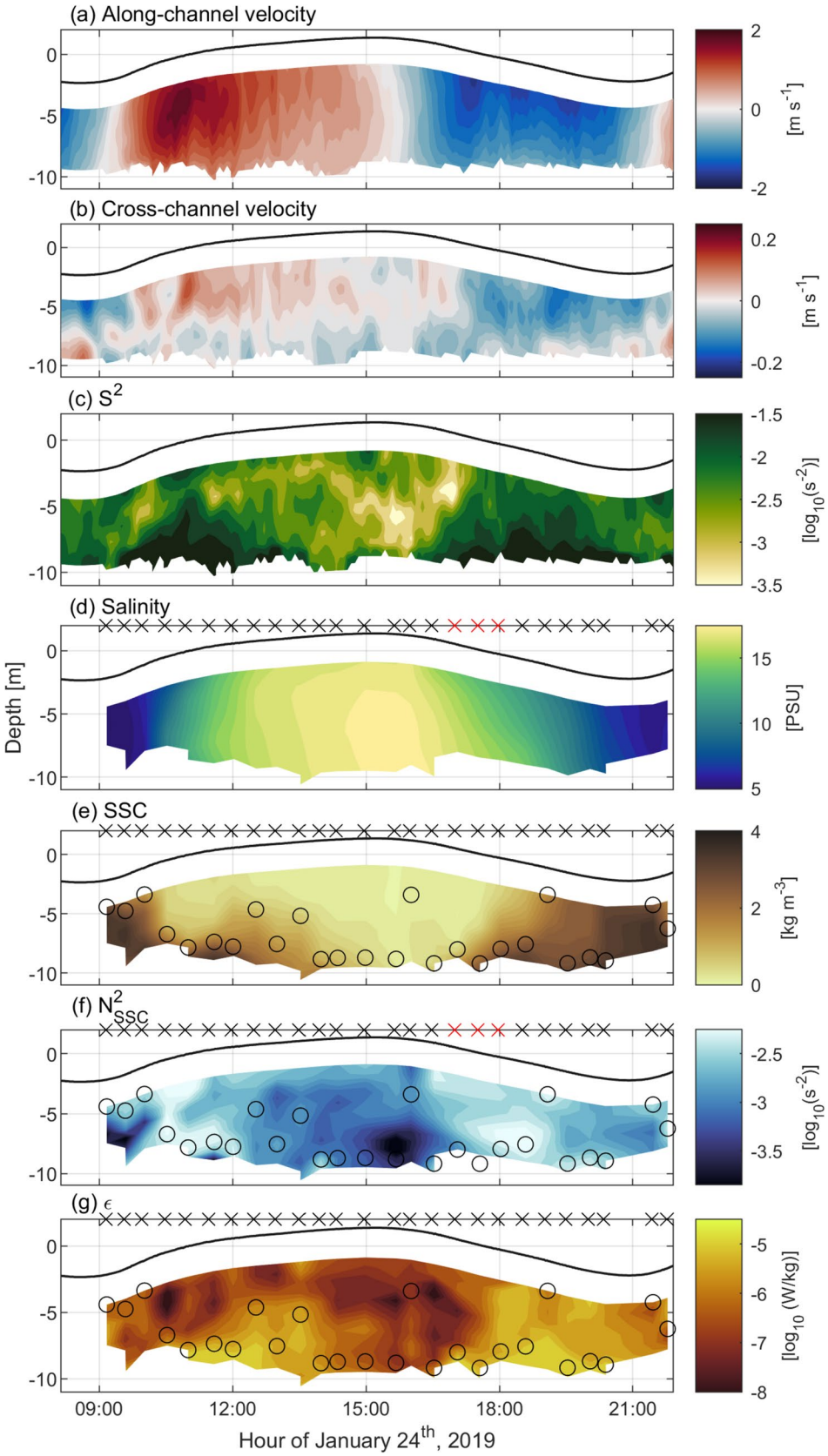

Fig. 3 Same as Fig. 2, but for the January 24, 2019, tidal cycle survey. The x's in red denote data that were interpolated

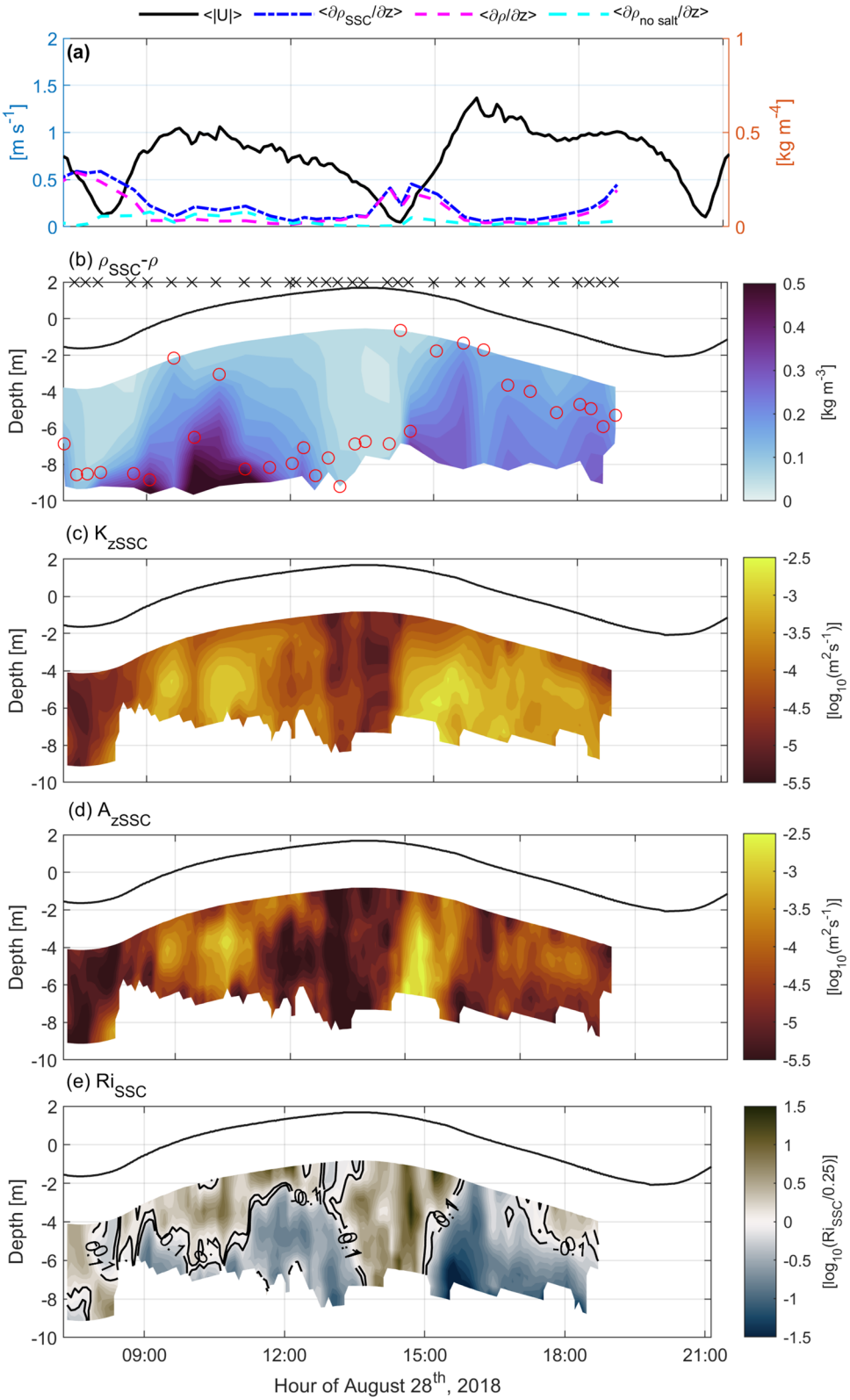

Fig. 4 (**a**) A depth-average of: the absolute value of the along-channel velocity (solid, black; left axis), the vertical gradient of the density including effects of SSC (dashed-dot, blue; right axis, units kg/m^4), the vertical gradient of density without the effects of SSC (magenta, dashed; right axis, units kg/m^4) and the vertical gradient of density excluding the effects of salinity (cyan, dashed; right axis, units kg/m^4) on August 28, 2018. With depth on the vertical axis: (**b**) The difference between density in terms of SSC and density without SSC. Contour levels depict increments of 0.1 kg/m^3. (**c**) Vertical eddy diffusivity using density in terms of SSC in the definition of the mixing efficiency of K_Z. (**d**) Vertical eddy viscosity using density in terms of SSC in the definition of the mixing efficiency of A_Z. (**e**) The Richardson number includes effects of SSC on density. Note panels (c), (d), and (e) are on a $\log_{10}$ scale

– ρ; Fig. 4b) mirrors the trend of the SSC measurements and the depth locations of maximum vertical gradients in SSC (Fig. 3e), illustrating the times and locations in the water column where the density is stabilized by the sediment. The vertical eddy diffusivity, K_{ZSSC}, and the vertical eddy viscosity, $A_{ZSSC,}$ (Fig. 4c-d) are highest when the difference

between the densities (ρ_{SSC}—ρ) is greatest, notably at peak flood tide (~ 9.5–10.5 h) and throughout ebb (~ 14-18 h). This indicates that elevated tidal shear induces mixing, which enhances the suspension of sediment, and therefore enhances the contribution of sediment to the density.

During peak flood and at the start of ebb (~ 15 h), A_{ZSSC} is greater than K_{ZSSC}, suggesting that there is greater mixing of momentum than diffusion, due to relatively low SSCs. Based on Eq. 5, $K_{ZSSC}/A_{ZSSC} < 1$ suggests that Ri_{SSC} must be less than 0.25 ($\log_{10}(Ri_{SSC}/0.25) = 0$), a value indicative of turbulence generation. This is contrary to the actual Ri_{SSC} (Fig. 4e), which suggests that the pycnocline inhibits mixing above depths of ~ 6 m on flood, and throughout the observed water column during early ebb.

January 2019

During January, $\langle \frac{\partial \rho_{SSC}}{\partial z} \rangle$, $\langle \frac{\partial \rho}{\partial z} \rangle$, and $\langle \frac{\partial \rho_{nosalt}}{\partial z} \rangle$ are largest during the peak tidal phases (Fig. 5a). Larger vertical salinity gradients during the January campaign compared to August are a result of larger river inflow (Fig. 2d, Fig. 3d), which is also responsible for the shift in the ETM position downstream (van Maren et al. 2023) and therefore larger $\langle \frac{\partial \rho_{nosalt}}{\partial z} \rangle$. Salinity-induced straining of density at the beginning of flood (~ 10–11 h) results in peaks in $\langle \frac{\partial \rho}{\partial z} \rangle$ and $\langle \frac{\partial \rho_{SSC}}{\partial z} \rangle$, however $\langle \frac{\partial \rho_{SSC}}{\partial z} \rangle$ remains elevated above $\langle \frac{\partial \rho}{\partial z} \rangle$ in the following hours due to large $\langle \frac{\partial \rho_{nosalt}}{\partial z} \rangle$, induced by resuspension of sediment by tidal shear.

The difference between ρ_{SSC} and ρ (Fig. 5b) is largest throughout the water column during low water slack into early flood tide (~ 9–10.5 h) and at the end of ebb tide (~ 20–22 h), corresponding to low S^2 (Fig. 3g). This suggests that at those times, the enhancement of the density by SSC is not a result of resuspension of sediment by tidal shear, but instead a result of sediment supplied to the midwater column by the nearby ETM. K_{ZSSC} (Fig. 5c) and A_{ZSSC} (Fig. 5d) are both low during peak flood (~ 10^{-5} m^2/s; ~ 10.5 h) at depths above ~ 7 m, indicating that vertical mixing is limited to near-bottom. At the same time, the Ri_{SSC} shows values around the critical threshold of 0.25 ($\log_{10}(Ri/0.25) = 0$) down to ~ 7 m (Fig. 5e), suggesting that low values of K_{ZSSC} and A_{ZSSC} above this depth are due to suppression of mixing by buoyancy. The sediment gradient, established by resuspension due to tidal shear, is strongest at this time (Fig. 5a) and contributes to the stratification that acts to confine mixing to the lower part of the water column. The mixing terms, K_{ZSSC} and A_{ZSSC}, are relatively high throughout much of the water column in the hours following peak flood (~ 12–14 h), particularly near bottom, reaching ~ 10^{-3} m^2/s at ~ 9.5 m and at ~ 13.8 h, with similar values observed during ebb. Understanding when sediment gradients impact the buoyancy, mixing and hydrodynamics of the Ems Estuary, in particular when the ETM is near its downstream limit (January), will be further elaborated upon in the discussion to follow.

Discussion

When does Sediment Influence Mixing?

The Ri_{SSC} can be compared to the Richardson number, Ri, quantified without SSC in the density to understand when in the tidal cycle sediment gradients have the most influence on mixing via density stratification (Fig. 6). In the region of the water column where sediment acts to stabilize the density, the buoyancy frequency N^2 without sediment may be negative, and therefore Ri is negative. Negative values of Ri and Ri_{SSC} have been removed and are not shown in Fig. 6. Negative values that persist in Ri_{SSC} indicate instability which may be caused by the advection of denser water over lighter water or by density overturning due to shear instability, although there are few instances of negative Ri_{SSC}, indicating that the water column is generally stabilized by sediment. Considering only stable values of the Ri, values above the critical threshold indicate where salinity-induced density stratification is sufficient to suppress turbulent mixing, without the contributions from SSC. Ri_{SSC} values above the threshold show regions in the water column where sediment acts to enhance the density stratification to levels sufficient to impact mixing.

Although SSCs were lower (< 1 kg/m^3) in August compared to January (> 3.5 kg/m^3), both datasets reveal that sediment increases the Richardson number at peak flood tide (Fig. 6), when suspension of sediment by tidal shear is maximum and sediment gradients are observed (Figs. 2e and 3e). In August, the influence of salinity on density overshadows that of the influence of SSC, which is apparent due to the thresholds of Ri_{SSC} and Ri nearly converging except for when SSC is highest during flood tide (~ 10-11 h, Figs. 6a-b). In January, the region surrounding the threshold of Ri_{SSC} extends several meters below that surrounding Ri throughout most of the flood phase (Fig. 6c-d), whereas during flood tide in August, the Ri and the Ri_{SSC} are nearly consistent (Fig. 6a-b). This indicates that during flood tide in January, sediment gradients play a role in the suppression of mixing by enhancing density stratification solely due to salt and temperature. The greater impact of SSCs in January compared to August is due to larger sediment concentrations caused by the closer proximity of the ETM. As shown by Zhu et al. (2021), vertical sediment-induced density gradients suppress mixing, which in turn enhances vertical gradients of SSCs, confining high concentrations to the lower part of the water column. This is more pronounced at higher sediment concentrations and is one mechanism that leads to the trapping of sediment (Zhu et al. 2021). In addition to the

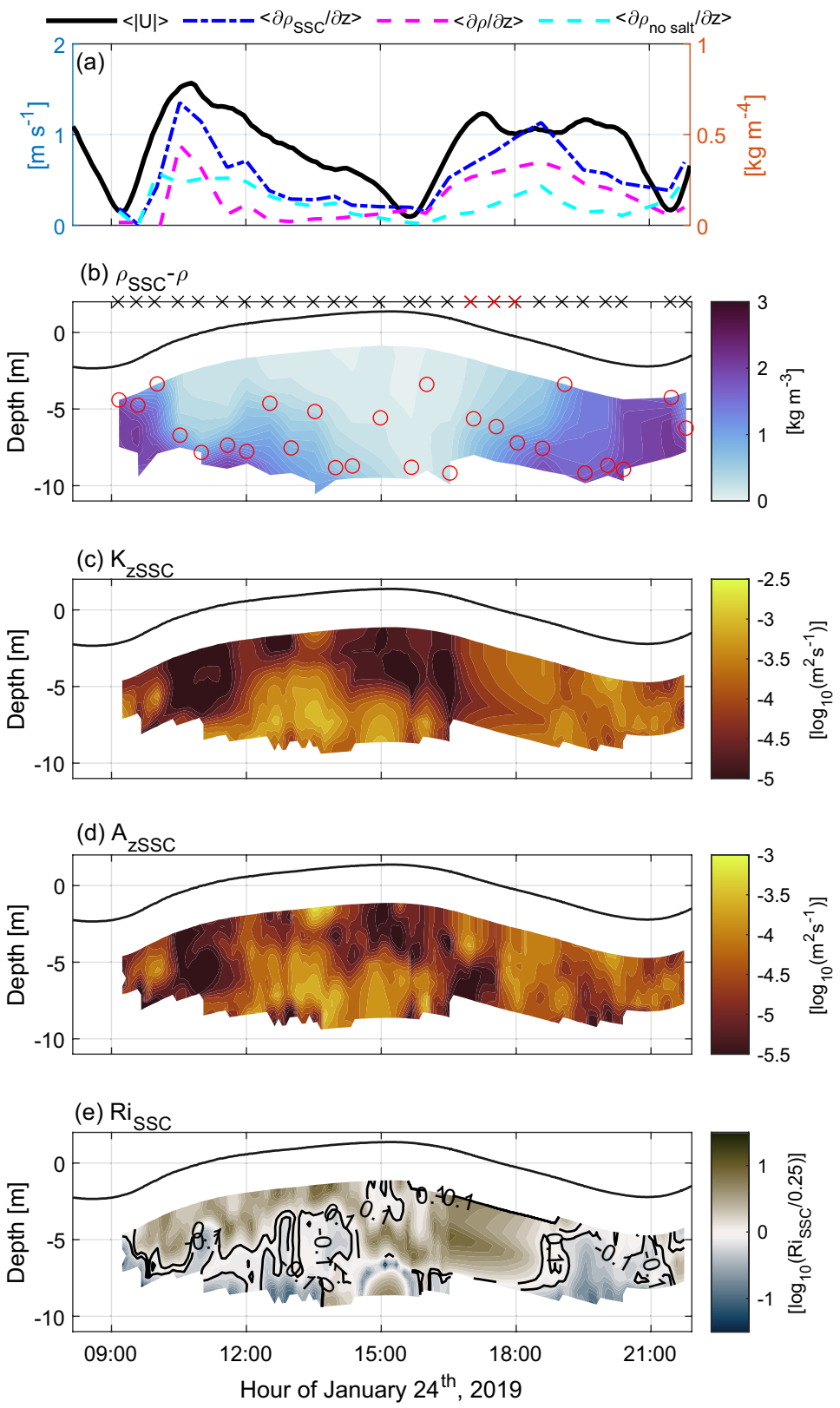

Fig. 5 (**a**) A depth-average of: the absolute value of the along-channel velocity (solid, black; left axis), the vertical gradient of the density including effects of SSC (dashed-dot, blue; right axis, units kg/m^4), the vertical gradient of density without the effects of SSC (magenta, dashed; right axis, units kg/m^4) and the vertical gradient of density excluding the effects of salinity (cyan, dashed; right axis, units kg/m^4) on January 24, 2019. With depth on the vertical axis: (**b**) The difference between density in terms of SSC and density without SSC. Contour levels depict increments of 0.15 kg/m^3. (**c**) Vertical eddy diffusivity using density in terms of SSC in the definition of the mixing efficiency of K_Z. (**d**) Vertical eddy viscosity using density in terms of SSC in the definition of the mixing efficiency of A_Z. (**e**) The Richardson number includes effects of SSC on density. Note that salinity measurements that were interpolated to fill a gap from 16.5 h to 19 h were used in K_{ZSSC}, A_{ZSSC}, and Ri_{SSC}. Bad cast data are denoted by red x's in panel (b). Panels (c), (d), and (e) are on a $\log_{10}$ scale

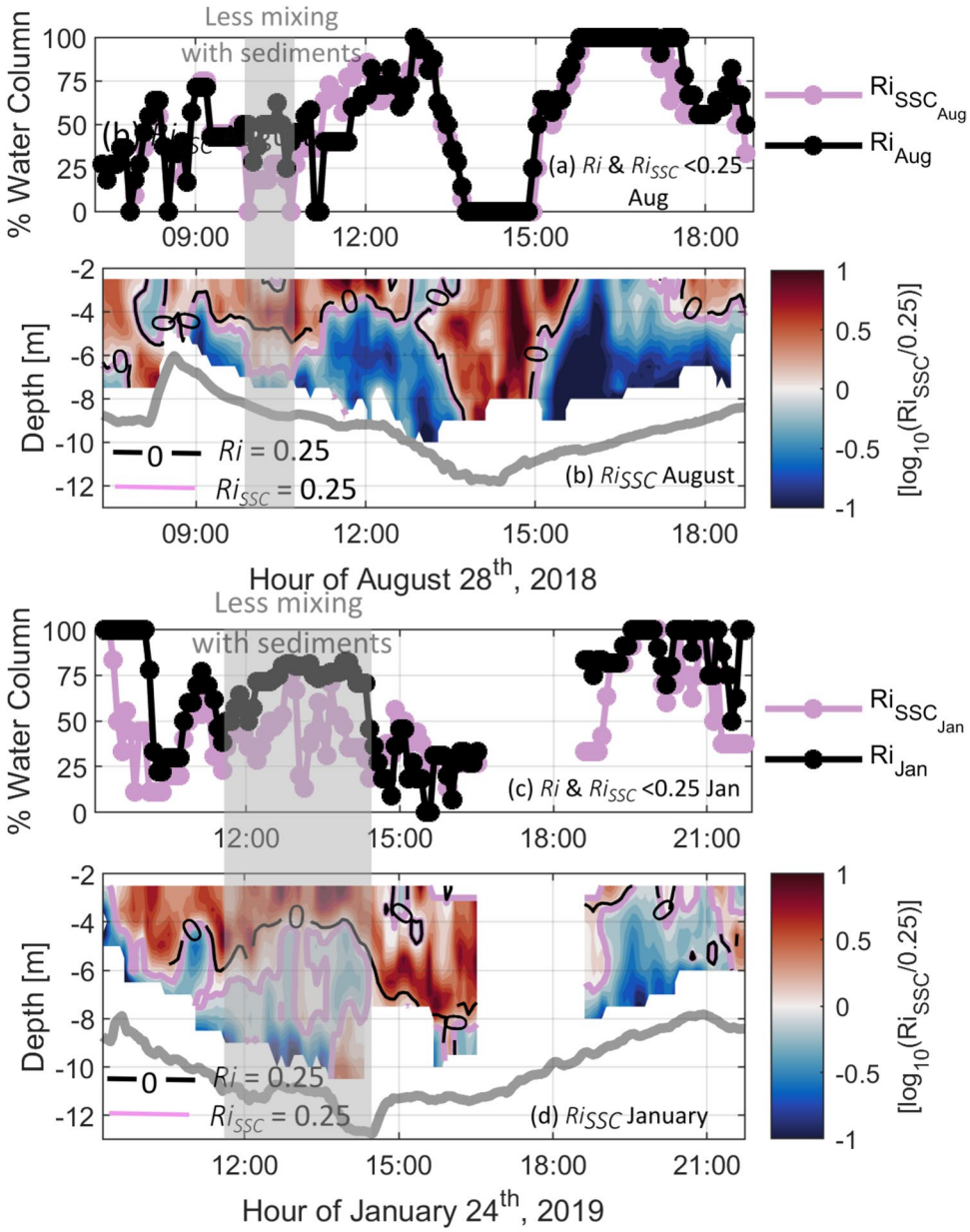

Fig. 6 (**a**) Percent of the water column where mixing takes place (percent of depth cells where *Ri* (black line) or Ri_{SSC} (purple line) < 0.25) in August 2018 and (**b**) depth and time variability of Ri_{SSC} for August 2018. Red depicts regions where mixing is expected to be suppressed by stratification ($Ri_{SSC} > 0.25$) and blue regions are where mixing is expected to occur ($Ri_{SSC} < 0.25$). The thick purple line denotes the contour level where $Ri_{SSC} = 0.25$, which surrounds the critical threshold indicative of suppression of mixing. The black contour line at 0 shows where $Ri = 0.25$ to reference the deviations from $Ri_{SSC} = 0.25$ (thick purple line). Subplots (c) and (d) are the same as (a) and (b) but for January 2019

importance of this for ETM formation in high-concentration areas (Zhu et al. 2021), the present findings suggest that this mechanism might also be important for generating sediment induced stratification capable of suppressing mixing at locations outside the ETM, where SSCs vary due to changes in the ETM location. It follows that the along-channel location of an upstream ETM is relevant for accurate representation of local vertical mixing dynamics downstream.

We would like to note that the intratidal variability of SSC during the January 2019 field campaign remarkably resembles that observed just downstream of our measurement location around a decade earlier by van Leussen (2011; their Fig. 3). Their measurements over a tidal cycle under relatively low river discharge conditions (~ 10–25 m^3/s) also depict a vertical sediment gradient on flood tide, which may have limited the vertical advection of SSC. They also found a more homogenous water column with SSCs extending to the surface during ebb tide, resembling that which we see in our observations and attribute to SSC sourced from the ETM upstream. However, SSCs measured by van Leussen (2011), around 1 kg/m^3 near bottom, are slightly lower than the January 2019 observations (~ 3 kg/m^3), which can likely be attributed to the increased turbidity of this area over the past decade as well as the location being further away from the ETM than our study.

Impacts of Temporal Variations in SSCs on Local Mixing Dynamics

Considering that the influence of sediment on density stratification was most pronounced during flood tide in January, the impact of tidal variations in SSCs on vertical mixing during the January measurements will be discussed. Typically, SIPS reduces mixing during ebb due to straining of the isohalines (Simpson et al. 1990; Jay 2010). During the January 2019 tidal cycle, straining of the isohalines occurred during early flood, creating density stratification that was enhanced near-bottom by the sediment gradient (see salinity and N^2_{SSC}; Fig. 3d and f). The sediment gradient was formed by local suspension of sediment by maximum tidal currents (~ 1.9 m/s), and contributed to stratification, as suggested by Ri_{SSC} (Fig. 6c-d). This sediment-enhanced density stratification caused vertical mixing to be confined to the lower water column during max flood. In the absence of salinity-induced density straining, it is possible that mixing during peak flood would have weakened the vertical sediment gradient by mixing sediment higher in the water column, providing greater opportunity for sediment advection away from the site by strong flood currents. These observations lend support to those of Zhu et al. (2021) which suggest that the effects of sediment-induced density gradients are more important when salinity stratification also affects the flow.

Becker et al. (2018) noted that in highly turbid systems the local density and flow structures are not controlled by salinity, but by SSC. The results of the present study suggest that in locations with lower SSCs, sediment can also play an important role in density structure, and hence in the mixing and flow dynamics, having consequences for sediment transport. Measurements in a shallow tidal channel in the Ems Dollard led Van der Ham et al. (2001) to suggest that the effects of sediment-induced stratification on sediment transport might not be important in shallow reaches in estuaries. Their conclusion was based on observations that showed minimal impact of sediment-induced stratification on turbulence when flow velocities were largest, which is when sediment transport rates are generally highest. The results of the present study suggest that this conclusion might not be relevant in deeper portions of the estuary, such as the Ems fairway. In the present study, suspended sediment was found to have the greatest impact on density stratification and mixing during peak flood tide in January, when SSCs were high due to the proximity of the upstream ETM. Sediment-enhanced stratification reduced mixing under max current velocities and limited the vertical suspension of SSC, possibly reducing the duration and extent of sediment import at this location in the Ems fairway.

The differences in local dynamics observed at the measurement site between August and January were a result of a change in sediment concentrations due to the shift in the along-channel position of the ETM. The differences between the August (relatively low SSCs) and January (relatively high SSCs) regimes can be further generalized as illustrated in Fig. 7. Vertical mixing rates increase under higher current velocities due to enhanced vertical shear. In conditions with "low" SSCs, weak sediment gradients are broken down by vertical mixing. In conditions with "high" SSCs, the sediment concentration impacts density stratification, stabilizing the water column. That is, high current velocities suspend sediments, which enhance density stratification in the water column. In turn, elevated density stratification suppresses vertical mixing, which further enhances the density gradient via settlement of sediment. Enhanced near-bottom stratification is also known to further enhance velocity shear in the water column (Adams and Weatherly 1981; Scully and Friedrichs 2003).

The processes summarized in Fig. 7, however, depend on several factors, including the local flow conditions and sediment properties. Implicit in Fig. 7 is the existence of a timescale over which A_{ZSSC} breaks down density stratification, which will vary depending on the strength of mixing and of stratification. Nonetheless, these results highlight the relevance of along-channel ETM position to locations downstream, as the ETM can alter local sediment concentrations and mixing dynamics.

Implications for other Estuaries

The results of the January 2019 campaign showed that SSCs enhanced density stratification on flood tide and suppressed A_{ZSSC} and K_{ZSSC}, a mechanism that did not noticeably impact mixing in August 2018, when sediment concentrations were relatively low. This variability in the effect of sediment on the density was due to the closer proximity of the ETM to the study site during January, suggesting that intratidal asymmetry in vertical mixing from sediment-induced stratification depends on the along-channel position of the ETM, even in locations not generally characterized as highly turbid. Such intratidal asymmetry in stratification will have implications for residual circulation, especially in the case of the Ems as buoyancy effects are more pronounced during flood tide, inverse to the classical estuarine circulation (Jay 2010). Because classical estuarine circulation results in sediment import (van Maren et al. 2015a), a change in the direction of sediment transport could result in this case.

The observation of greater vertical sediment gradients on flood versus ebb tide during both August and January, which contribute to buoyancy and enhance the Richardson number on flood tide, are consistent with observations in the macrotidal Qiantang estuary (Tu et al. 2019). However, sediment concentrations observed by Tu et al. (2019) were higher than those observed here, up to 15 kg/m^3 near the bed. In their study in the north passage of the Changjiang

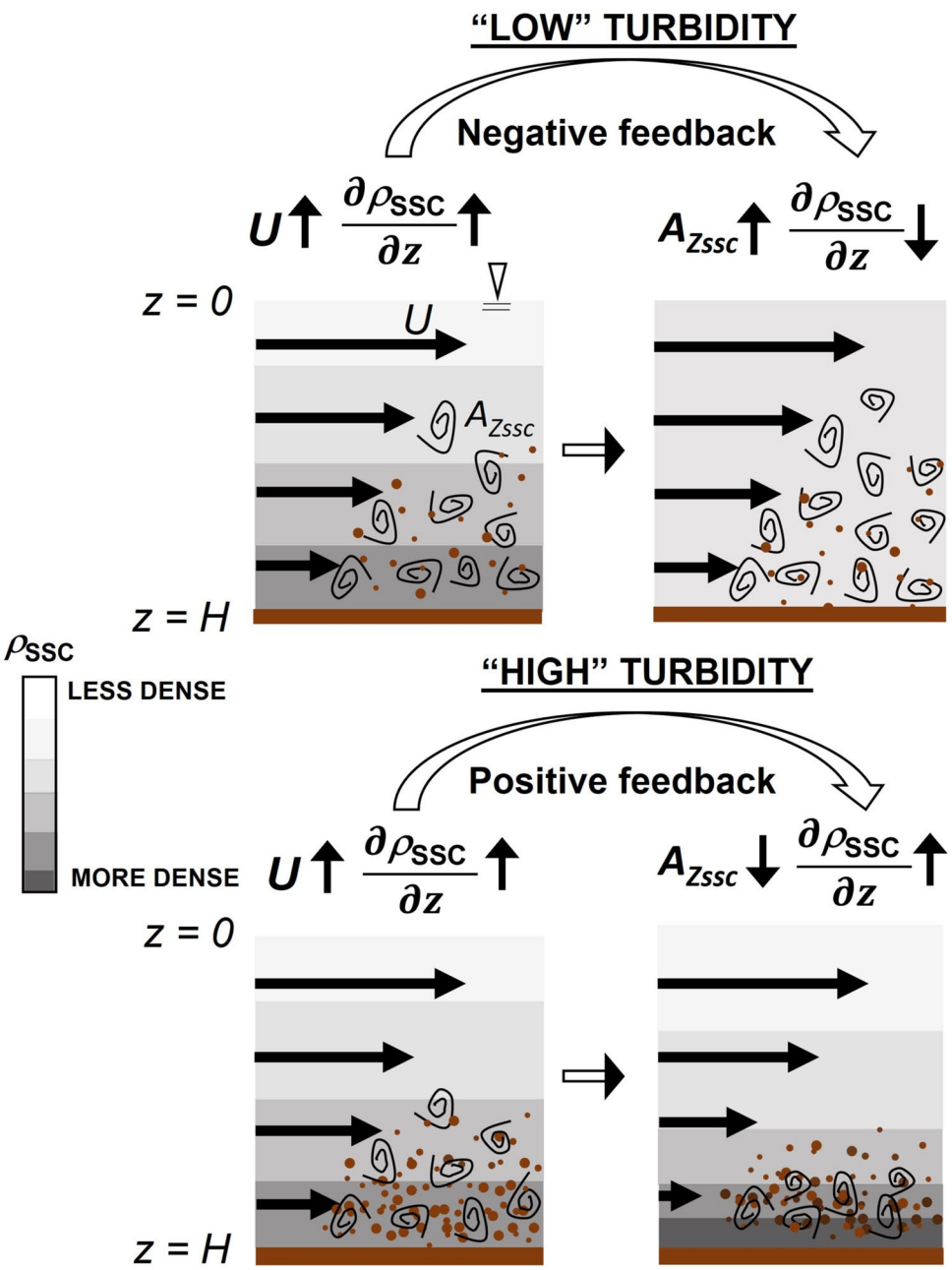

Fig. 7 Illustration of the impact of suspended sediment concentration on the vertical density gradient and mixing. Top: when turbidity is relatively "low", maximum tidal currents increase the vertical density gradient due to elevated suspended sediment concentration, but mixing is also enhanced (Az_{SSC}) which acts to homogenize the water column. Bottom: When turbidity is relatively "high", the maximum tidal currents will again enhance vertical density gradients by suspending sediment in the water column, however the enhanced density gradients then act to suppress mixing which then further enhances the vertical density gradient

Estuary, Niroomandi et al. (2018) showed that sediment-induced stratification may reduce vertical eddy viscosity in the water column by 10–30%. Their data was collected during a spring and neap tide at several locations along the channel with varying SSCs (on the order of 10^{-2} to 10^{2} kg/m^3) near bottom. Despite differences in concentrations, the results of the present study support the general findings in the Qiantang estuary by Tu et al. (2019) and in the Changjiang Estuary by Niroomandi et al. (2018), that sediment-induced stratification contributes to reduction but not total suppression of turbulent mixing, but show that this phenomenon can occur in systems with much lower SSCs than previously studied. A consequence of reduced mixing on flood tide, as observed in the present study, is the limited vertical extent of SSC in the water column, of particular importance during peak flood when currents are strongest and the potential for upstream flux of sediment is therefore greatest. It follows that at the measurement location in the Ems fairway, a reduction of sediment import might be observed when local SSCs are high enough to impact density stratification, like they were in January due to the proximity of the ETM.

At the location of an ETM in the south passage of the Changjiang Estuary, and under similar SSCs as this study

(~0–5 kg/m^3), Lu et al. (2020) also showed that salinity-induced stratification and sediment-induced stratification jointly reduce turbulence. Salinity-induced stratification in the upper part of the water column was shown to dampen turbulence and inhibit vertical suspension of sediment, which increased sediment concentration gradients below. Increased SSC gradients acted to further suppress turbulence, confining sediment to the near-bottom layer. This combined effect of salinity- and sediment-induced stratification essentially traps sediments near bottom, causing sediment to accumulate, attributing to ETM formation (Lu et al. 2020). However, Lu et al. (2020) observed strongest stratification when current velocities were low at the early tidal phases, particularly flood tide, and when salinity gradients were strongest in the upper and mid-water column. Although the results of the present study also suggest that the effects of sediment gradients are more important in the presence of overlying salinity-induced stratification, the dynamics in the Changjiang Estuary differ from those observed in the Ems fairway where sediment gradients were generated by resuspension during strong tidal currents at max flood tide. Further, given the importance of salinity gradients to the dynamics described above, the lateral flow dynamics may also play an important role, a topic that should be investigated in future studies.

Limitations of this Study and Considerations to the Local Dynamics

Local sediment properties and concentrations vary due to a range of factors, even within a single system. The measurements presented here, which were conducted over two semidiurnal tidal cycles at the same location, but under varying river discharge conditions, are an example of this. Considering the findings of previous studies, the magnitude and properties of the sediment concentrations likely influence the impact of temporal variations in SSCs on local mixing dynamics (Winterwerp 2001; Becker et al. 2018; Moodie et al. 2022). In conditions of fluid mud, settlement and thus restratification of the fluid mud layer, preceded by breakdown due to tidal mixing on flood, occurs when tidal currents are relatively weak (Becker et al. 2018). However, in conditions of lower sediment concentrations, when fluid mud is not present, sediment-induced stratification appears to form in the water column under maximum tidal currents, when suspension of SSC by tidal currents is possible (Scully and Friedrichs 2003; Tu et al. 2019; and the present study). In general, assessment of the magnitude of local sediment concentrations might help to predict when, relative to the tidal phase, the contribution of SSC to the buoyancy is greatest. Assessment of the sediment properties at this measurement location is beyond the scope of the present study. Without this and considering only a single measurement location with temporal variability, it is not possible to determine the quantity of the suspended sediment that settled at the measurement location versus what was advected away from the measurement site. Future studies are encouraged to collect current velocity, SSC, mixing and density data over an estuarine cross-section for full tidal cycles to have a better understanding of the impact of SSCs on mixing and sediment transport.

It should also be re-emphasized that both measurement campaigns were conducted during spring tides. Neap tides, which correspond to weaker tidal currents, might not experience the same magnitude of sediment suspension, and therefore vertical sediment gradients that strengthened the density gradient. Weaker stratification would ultimately lead to less suppression of turbulence and mixing. It follows that under neap tide conditions, the local dynamics described here as they pertain to sediment transport may be less important.

Conclusions

This study investigated the relevance of the along-channel position of an upstream ETM on local hydrodynamics and vertical mixing dynamics in the Ems Estuary. For this investigation, in-situ data collected during a tidal cycle when the ETM was 25 km upstream (August 2018) and 5 km upstream (January 2019) of the measurement site were analyzed. During the August 2018 campaign salinity dominated the density structure and suspended sediment had little influence on vertical mixing. During the January 2019 campaign SSCs were elevated compared to August due to the ETM proximity. Under these conditions, the gradient Richardson number indicated that sediment gradients contributed to density stratification established by salinity, capable of suppressing mixing on flood tide. At peak flood tide turbulence and vertical mixing were limited to the lower part of the water column, resulting in tidal asymmetries in mixing.

ETMs can exhibit seasonal and tidal variability in along-channel position. It was shown in the present study that sufficient sediment gradients in the lower water column can enhance density stratification and contribute to the dampening of turbulence. It follows that variability in along-channel position of an ETM is relevant to accurately describe local vertical mixing dynamics downstream, due to its capacity to supply sediment that can impact buoyancy. Increases in sediment concentrations were found to alter local mixing dynamics by increasing density stratification. Under strong currents, larger density gradients were established by sediment resuspension, which enhanced the dampening of turbulence and further increased stratification. These local dynamics are important because they may ultimately impact residual flows and sediment transport in estuaries.

Supplementary Information The online version contains supplementary material available at https://doi.org/10.1007/s12237-024-01438-4.

Acknowledgements We would like to thank Preston Spicer for aiding with the field data collection for this study. We would also like to thank Dr. Kimberly Huguenard for advice on data analysis and Dr. Aldo Sottolichio for providing insights into turbidity calibration. Lauren Ross would like to acknowledge funding from the NSF Grant Number 2045866 that aided in the completion of this study. All data used in this study are available in van Maren et al. (2023). We thank reviewers Huib de Swart, Qian Yu, and one anonymous reviewer for their constructive feedback that greatly aided the manuscript.

Data Availability Statement All data used in this study are described in van Maren et al. (2023) and are available at https://doi.org/https://doi.org/10.4121/c.6056564.v3.

References

Adams, C., and G.L. Weatherly. 1981. Suspended-Sediment Transport and Benthic Boundary-Layer Dynamics. *Developments in Sedimentology* 32: 1–18.

Becker, M., C. Maushake, and C. Winter. 2018. Observations of mud-induced periodic stratification in a hyperturbid estuary. *Geophysical Research Letters* 45 (11): 5461–5469.

Chernetsky, A.S., H.M. Schuttelaars, and S.A. Talke. 2010. The effect of tidal asymmetry and temporal settling lag on sediment trapping in tidal estuaries. *Ocean Dynamics* 60 (5): 1219–1241.

De Jonge, V.N., H.M. Schuttelaars, J.E.E. van Beusekom, S.A. Talke, and H.E. de Swart. 2014. The influence of channel deepening on estuarine turbidity levels and dynamics, as exemplified by the Ems estuary. *Estuarine, Coastal and Shelf Science* 139: 46–59. https://doi.org/10.1016/j.ecss.2013.12.030.

Dijkstra, Y.M., H.M. Schuttelaars, G.P. Schramkowski, and R.L. Brouwer. 2019. Modeling the transition to high sediment concentrations as a response to channel deepening in the Ems River Estuary. *Journal of Geophysical Research: Oceans* 124 (3): 1578–1594.

Douglas, W.R., R. Lueck, and J. McMillan. 2018. *ODAS MATLAB library technical manual version 4.3*. Rockland Scientific International Inc. www.rocklandscientific.com. Accessed 1 Sept 2020.

Dyer, K.R., M.C. Christie, N. Feates, M.J. Fennessy, M. Pejrup, and W. van der Lee. 2000. An Investigation into Processes Influencing the Morphodynamics of an Intertidal Mudflat, the Dollard Estuary, The Netherlands: I. Hydrodynamics and Suspended Sediment. *Estuarine, Coastal and Shelf Science* 50 (5): 607–625. https://doi.org/10.1006/ecss.1999.0596.

Dyer, K.R., M.C. Christie, and A.J. Manning. 2004. The effects of suspended sediment on turbulence within an estuarine turbidity maximum. *Estuarine, Coastal and Shelf Science* 59: 237–248.

Efron, B., and G. Gong. 1983. A leisurely look at the bootstrap, the jackknife and cross-validation. *The American Statistician* 37: 36–48.

Esri. 2024. Imagery Hybrid. https://www.arcgis.com/home/item.html?id=86265e5a4bbb4187a59719cf134e0018. Accessed 7 Aug 2024.

Fettweis, M., R. Riethmüller, R. Verney, M. Becker, J. Backers, M. Baeye, M. Chapalain, S. Claeys, J. Claus, T. Cox, J. Deloffre, D. Depreiter, F. Druine, G. Flöser, S. Grünler, F. Jourdin, R. Lafite, J. Nauw, B. Nechad, R. Röttgers, A. Sottolichio, T.V. Engeland, W. Vanhaverbeke, and H. Vereecken. 2019. Uncertainties associated with in situ high-frequency long-term observations of suspended particulate matter concentration using optical and acoustic sensors. *Progress in Oceanography* 178: 102162. https://doi.org/10.1016/j.pocean.2019.102162.

Guan, W.B., S.C. Kot, and E. Wolanski. 2005. 3-D fluid-mud dynamics in the Jiaojiang Estuary, China. *Estuarine, Coastal and Shelf Science* 65: 747–762. https://doi.org/10.1016/j.ecss.2005.05.017.

Huguenard, K.D., A. Valle-Levinson, M. Li, R.J. Chant, and A.J. Souza. 2015. Linkage between lateral circulation and near-surface vertical mixing in a coastal plain estuary. *Journal of Geophysical Research: Oceans* 120: 4048–4067. https://doi.org/10.1002/2014JC010679.

Jay, D.A. 2010. Estuarine Variability. In *Contemporary Issues in Estuarine Physics*, ed. A. Valle-Levinson, 145–185. Cambridge, United Kingdom: Cambridge University Press.

Kay, D.J., and D.A. Jay. 2003. Interfacial mixing in a highly stratified estuary: 1. Characteristics of mixing. *Journal of Geophysical Research* 108 (C3): 3072. https://doi.org/10.1029/2000JC000252.

Lu, T., H. Wu, F. Zhang, J. Li, L. Zhou, J. Jia, Z. Li, and Y.P. Wang. 2020. Constraints of salinity-and sediment-induced stratification on the turbidity maximum in a tidal estuary. *Geo-Marine Letters* 40: 765–779.

Lueck, R., E. Murowinski, and J. McMillan. 2020. *A Guide to Data Processing (RSI Technical Note 039)*. Victoria, BC, Canada: Rockland Scientific Inc.

McDougall, T.J., and P.M. Barker. 2011. Getting started with TEOS-10 and the Gibbs Seawater (GSW) Oceanographic Toolbox. *SCOR/IAPSO WG* 127: 1–28.

Miles, J.W. 1961. On the stability of heterogeneous shear flows. *Journal of Fluid Mechanics* 10: 496–508.

Moodie, A.J., J.A. Nittrouer, H. Ma, B.N. Carlson, Y. Wang, M.P. Lamb, and G. Parker. 2022. Suspended sediment-induced stratification inferred from concentration and velocity profile measurements in the Lower Yellow River, China. *Water Resources Research* 58 (5): e2020WR027192.

Niroomandi, A., G. Ma, S.F. Su, F. Gu, and D. Qi. 2018. Sediment flux and sediment-induced stratification in the Changjiang Estuary. *Journal of Marine Science and Technology* 23: 349–363.

Osborn, T.R. 1980. Estimates of the Local Rate of Vertical Diffusion from Dissipation Measurements. *Journal of Physical Oceanography* 10: 83–89.

Papenmeier, S., K. Schrottke, A. Bartholomä, and B.W. Flemming. 2013. Sedimentological and rheological properties of the water–solid bed interface in the Weser and Ems estuaries, North Sea, Germany: Implications for fluid mud classification. *Journal of Coastal Research* 29 (4): 797–808.

Ross, L., K.D. Huguenard, and A. Sottolichio. 2019. Intratidal and fortnightly variability of vertical mixing in a macrotidal estuary: The Gironde. *Journal of Geophysical Research: Oceans* 124: 2641–2659. https://doi.org/10.1029/2018JC014456.

Ross, M.A. 1988. Vertical structure of estuarine fine sediment suspensions. Ph.D. thesis, University of Florida, Gainesville, Florida, U.S.A. https://ufdc.ufl.edu/uf00075487/00001

Schulz, K., H. Burchard, V. Mohrholz, P. Holtermann, H.M. Schuttelaars, M. Becker, C. Maushake, and T. Gerkema. 2020. Intratidal and spatial variability over a slope in the Ems estuary: Robust along-channel SPM transport versus episodic events. *Estuarine, Coastal and Shelf Science* 243: 106902. https://doi.org/10.1016/j.ecss.2020.106902.

Scully, M.E., and C.T. Friedrichs. 2003. The influence of asymmetries in overlying stratification on near-bed turbulence and sediment suspension in a partially mixed estuary. *Ocean Dynamics* 53: 208–219. https://doi.org/10.1007/s10236-003-0034-y.

Simpson, J.H., J. Brown, J. Matthews, and G. Allen. 1990. Tidal straining, density currents, and stirring in the control of estuarine

stratification. *Estuaries* 13 (2): 125–132. https://doi.org/10.2307/1351581.

Spicer, P., and K. Huguenard. 2020. Observations of Near-Surface Mixing Behind a Headland. *Journal of Marine Science and Engineering* 8 (2): 68. https://doi.org/10.3390/jmse8020068.

Talke, S.A., and H.E. de Swart. 2006. *Hydrodynamics and Morphology in the Ems/Dollard Estuary: Review of Models, Measurements, Scientific Literature, and the Effects of Changing Conditions*. Institute for Marine and Atmospheric Research Utrecht (IMAU), Technical Report: University of Utrecht.

Talke, S.A., H.E. de Swart, and H.M. Schuttelaars. 2009. Feedback between residual circulations and sediment distributions in highly turbid estuaries: An analytical model. *Continental Shelf Research* 29: 119–135.

Thomson, R.E., and W.J. Emery. 2014. Data analysis methods in physical oceanography. *Elsevier Science*. https://doi.org/10.1016/C2010-0-66362-0.

Tjernstrom, M. 1993. Turbulence length scales in a stably stratified free shear flow analyzed from slant aircraft profiles. *Journal of Applied Meteorology* 32: 948–963.

Tu, J., D. Fan, Y. Zhang, and G. Voulgaris. 2019. Turbulence, sediment-induced stratification, and mixing under macrotidal estuarine conditions (Qiantang Estuary, China). *Journal of Geophysical Research: Oceans* 124: 4058–4077. https://doi.org/10.1029/2018JC014281.

Van der Ham, R., H.L. Fontijn, C. Kranenburg, and J.C. Winterwerp. 2001. Turbulent exchange of fine sediments in a tidal channel in the Ems/Dollard estuary. Part I: Turbulence measurements. *Continental Shelf Research* 21: 1605–1628.

Van Leussen, W. 2011. Macroflocs, fine-grained sediment transports, and their longitudinal variations in the Ems Estuary. *Ocean Dynamics* 61 (2): 387–401.

Van Maren, D.S., T. van Kessel, K. Cronin, and L. Sittoni. 2015a. The impact of channel deepening and dredging on estuarine sediment concentration. *Continental Shelf Research* 95: 1–14. https://doi.org/10.1016/j.csr.2014.12.010.

Van Maren, D.S., J.C. Winterwerp, and J. Vroom. 2015b. Fine sediment transport into the hyper-turbid lower Ems River: The role of channel deepening and sediment-induced drag reduction. *Ocean Dynamics* 65: 589–605. https://doi.org/10.1007/s10236-015-0821-2.

Van Maren, D.S., A.P. Oost, Z.B. Wang, and P.C. Vos. 2016. The effect of land reclamations and sediment extraction on the suspended sediment concentration in the Ems Estuary. *Marine Geology* 376: 147–157.

Van Maren, D.S., C. Maushake, J.-W. Mol, D. van Keulen, J. Jürges, J. Vroom, H. Schuttelaars, T. Gerkema, K. Schulz, T.H. Badewien, M. Gerriets, A. Engels, A. Wurpts, D. Oberrecht, A.J. Manning, T. Bailey, L. Ross, V. Mohrholz, D.M.L. Horemans, M. Becker, D. Post, C. Schmidt, and P.J.T. Dankers. 2023. Synoptic observations of sediment transport and exchange mechanisms in the turbid Ems estuary: The EDoM campaign. *Earth Syst. Sci. Data* 15 (1): 53–73.

Winterwerp, J.C. 2001. Stratification effects by cohesive and noncohesive sediment. *Journal of Geophysical Research: Oceans* 106 (C10): 22559–22574.

Winterwerp, J.C. 2011. Fine sediment transport by tidal asymmetry in the high-concentrated Ems River: Indications for a regime shift in response to channel deepening. *Ocean Dynamics* 61: 203–215. https://doi.org/10.1007/s10236-010-0332-0.

Winterwerp, J.C., Z.B. Wang, A. van Braeckel, G. van Holland, and F. Kösters. 2013. Man-induced regime shifts in small estuaries—II: A comparison of rivers. *Ocean Dynamics* 63 (11–12): 1293–1306. https://doi.org/10.1007/s10236-013-0663-8.

Winterwerp, J.C., J. Vroom, Z.B. Wang, M. Krebs, E.C.M. Hendriks, D.S. van Maren, K. Schrottke, C. Borgsmüller, and A. Schöl. 2017. SPM response to tide and river flow in the hyper-turbid Ems River. *Ocean Dynamics* 67: 559–583. https://doi.org/10.1007/s10236-017-1043-6.

Zhu, C., D.S. Van Maren, L. Guo, J. Lin, Q. He, and Z.B. Wang. 2021. Effects of sediment-induced density gradients on the estuarine turbidity maximum in the Yangtze Estuary. *Journal of Geophysical Research: Oceans* 126: e2020JC016927. https://doi.org/10.1029/2020JC016927.